Visualization of Steel Continuous Casting Including a New Integral Method for Post-Processing Temperature Data

*Matthew L. S. Zappulla, Seong-Mook Cho, and Brian G. Thomas**

Understanding and improving complex manufacturing processes such as steel continuous casting can have a tremendous global impact. Due to the extremely harsh environments, computational modeling is more important than ever in the study of these processes. Being able to visualize the model results in a manner that conveys accurate process understanding as well as being visually digestible can be difficult, especially for transient, three-dimensional models. Depending on the objective, it is also important to distinguish between graphically-pleasing and physically-based visualization. Following physically-based visualization guidelines can help make the model results easier to understand and interpret. Examples include: color maps based on temperature, glyphs to show multiple stress components, vector plots overlaying a scalar field, diverging and discrete color maps to differentiate tension and compression, and orienting figures so that gravity acts downwards. This paper explores methodologies for post processing, as well as the selection of some visualization parameters, for a variety of variables and models relevant to understanding and quantifying the complex phenomena in steel continuous casting. Finally a methodology is introduced for the processing of high-density data from temperature sensors to better visualize potential quality issues on the surface of a continuously cast slab.

1. Introduction

Progressive development of both models and advanced measurement technologies has enabled a better understanding of complex phenomena and defect formation mechanisms in mature manufacturing processes such as continuous steel casting. Models of continuous casting include many different types: online control systems, scheduling and cost models, finite-difference and -volume computational models of turbulent fluid flow, gas injection, electromagnetic fields, solidification, and finite-element models of thermal-mechanical behavior, taper, bulging between rolls, and soft reduction, just to name a few. In

addition to the results of sophisticated computational models, improvements in sensor technology and data collection also provide vast quantities of high resolution data faster every day. Understanding how to present and interpret this big data in a meaningful way can be a challenge.

Due to the difficulties of making measurements in the harsh environment of continuous steel casting, computational models are needed to understand the transient and complex physical phenomena that occur. In addition to models, when possible, plant measurements are important for verification and validation. Field variables such as temperature, velocity, pressure, displacement, strain, and stress are important to understanding behaviors in the process. Visualizing the three-dimensional (3D) spatial variations of the results of these variables in a 2D medium such as a journal paper is challenging, especially when the variations evolve with time, as most of the interesting transient phenomena governing real materials do. Finding effective ways to post process the results to visualize the phenomena is very problem specific. Prior process understanding can help to narrow down the important variables, orientations, and parameters to display that best convey the insights contained in the information.

Video animation is a helpful tool to enable understanding of complex transient phenomena during casting processes. A few previous studies have shown animated visualization of flow and defect mechanisms during continuous casting. Slag entrainment into the molten steel pool and slag entrapment due to sudden surface level drops, which can cause sliver defects in final steel products, was visualized through high-resolution animations of multiphase from Large Eddy Simulation (LES).[1] Transient jet behavior and alumina particle trajectories were visualized with validated LES videos.[2,3] The effects of single-ruler EMBr[4] and nozzle port design[5] on transient fluid flow during slab casting were studied by visualizing transient flow of molten metal in lab scale models. The transport of argon-bubbles inside a slab mold was animated with and without double-ruler EMBr, by compiling snapshots from LES coupled with a discrete phase model and MHD model.[6] Oscillation mark and hook formation, which greatly affects steel surface quality, was animated during a mold oscillation cycle, and

Prof. B. G. Thomas, M. L. S. Zappulla, Dr. S.-M. Cho
Mechanical Engineering
Colorado School of Mines
1500 Illinois St., Golden, CO, 80401, USA
E-mail: bgthomas@mines.edu

The ORCID identification number(s) for the author(s) of this article can be found under https://doi.org/10.1002/srin.201800540.

verified with sub-surface microstructure evolution using a variety of microanalysis techniques.[7,8]

This work focuses on visualization techniques to display 3D transient information in continuous casting of steel, including thermal fluid flow phenomena, solidification, and mechanical behavior in the mold region. In addition to displaying the results of computational models, a novel methodology is presented here to display high-density temperature data collected from an instrumented continuous casting mold that enables real-time visualization and prediction of surface defect formation.

2. Purpose Driven Visualization

The best visualization method depends on the objectives. If the objective is to entertain and inspire, or to show general trends, the ideal visualizations will be very different than if the goal is to accurately convey quantitative information. It is understood that within a publication, line-types, styles, and symbols for plotting a particular case should be consistent throughout the length. The display of abstract tensor variables such as stress should differ from the display of readily-observed scalar variables such as temperature, which can benefit from a physically-based visualization scheme.

The mesh resolution needed to convey results that are pleasing to the human eye often differs from what is best for numerical methods, and vice-versa. For example, a well refined and efficient finite-element mesh that yields good numerical accuracy for stress analysis throughout a given domain typically has a very biased mesh with large elements in most regions and tiny elements near corners, geometry changes, and areas of interest. Meshing that same domain for computer generated images for visualizing temperature or rendering light reflections, for example, would look substantially different.

It usually helps to pay attention to the underlying physics when visualizing data. For example, orienting the domain so that gravity always acts downwards usually makes it intuitively easier to understand the results. Bounding a color map according to limits that are physically achievable in the process is another way to make results easier to see. Maintaining the true aspect ratios of the part domain/geometry is always best, unless there is a good reason to distort the domain to focus on a particular result. Such physically-based visualizations convey the data in a way that is spatially accurate, and enables realistic interpretation to extract fundamental understanding needed to make process improvements easier to accomplish.

3. Grid/Mesh Visualization and Interpolation

For a model simulation, the first purpose of visualization should be to determine if the simulation results are reasonable. Most computational methodologies, including finite-volume and finite-element methods, involve a grid of cells or a mesh of the domain, and nodal points. The discretization boundaries between the cells/elements should be sufficiently refined as to have no influence on the results. If any vestige of the grid/mesh can be discerned in the results, this indicates a potential problem with the accuracy. Thus, it is often useful to overlay the grid/mesh onto contour plots of the field-variable results in order to distinguish real physical phenomena from mesh-related artifacts. Once the grid/mesh resolution has been established to be sufficient, and the results to be accurate, there is no need to plot the grid/mesh. Indeed, a properly-refined grid/mesh will typically will be too dense to see through, and showing it will likely distract the reader from the display of information.

Similarly, grid information can also benefit the initial display of measurements. Measured data in many engineering processes is now becoming dense enough to plot contour maps of field variables. However, if the distance between measurements is still too large, important phenomena may be missed, and the contours may not accurately represent the field variable being measured. Additionally, it is important to be able to troubleshoot sensor systems and identify anomalies in individual or groups of sensors. Showing the grid in the visualization can help with these issues.

Default settings for plots in many commercial packages, such as MATLAB,[9] often add grid spacing to the contour plots. In some cases this is desirable, such as shown in **Figure 1**a, where the grid discretization conveys the exact spatial locations of the collected temperature data. Other scenarios where this might be useful are when space is limited and showing the grid also conveys something about the finite element mesh resolution, such as during a mesh refinement study. When attempting to turn off the grid spacing in a program such as MATLAB, one should be wary of associated setting changes, which also affect the data displayed, such as shading: this is a common situation that often also turns on interpolation.

For both model results and measurements, it is best to plot values at the points of greatest accuracy (e.g., cell centers in finite-difference methods, integration points in finite-element results, and actual points from measured data) and then to connect them with straight lines. However, once a mesh is sufficiently refined that the contours, represented as line segments, appear smooth, plotting at other locations, such as at nodes, is acceptable Some post processing software performs non-linear interpolation between the actual calculated or measured points. This is often not appropriate, as it adds unintended artifacts to the displayed results, especially when the interpolation method does not match the model or data. While interpolation is usually intended to make smoother and more appealing visuals, this is actually a disservice because it obscures the real physical phenomena from mesh related artifacts. Deviations that would indicate accuracy problems due to an insufficiently-refined grid may be suppressed. Thus, using interpolation to suppress the "wiggles" is ill-advised.[10]

Moreover, minor glitches in the data sometimes become magnified by an inappropriate interpolation method. For example, in order to achieve a continuous curve, a cubic spline interpolation of data with a single outlying point may produce a kinked line that extends far outside the range of all of the data points. The resulting new extreme peaks may mislead the viewer to believe that some real physical behavior is responsible for a new trend that actually does not exist. To avoid such problems, the safest interpolation method, if a continuous line is desired, is to represent the real data points with symbols, and to connect them with straight lines. This accurately conveys the information without misleading the reader. This methodology is readily extended to visualize data in multiple dimensions, such as adding a third spatial dimension or time.
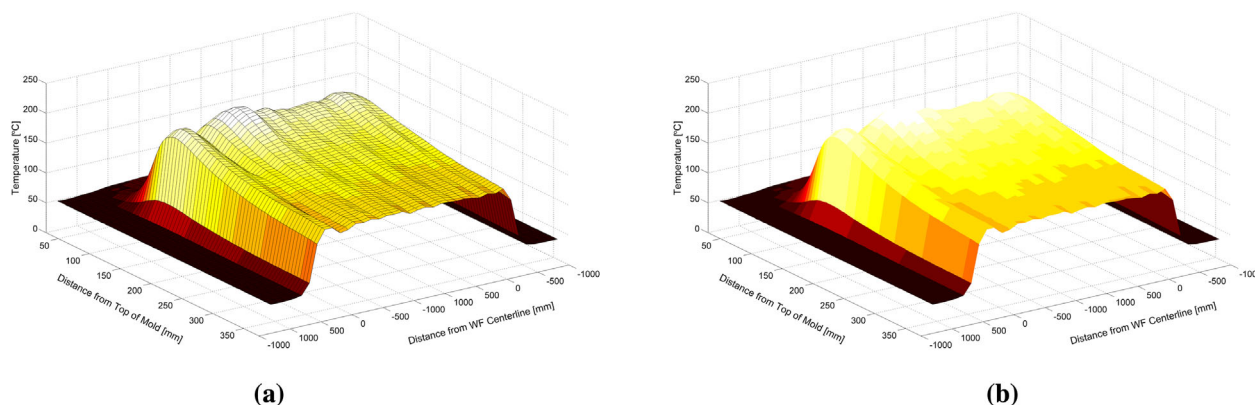
1800540 (2 of 11)

**ADVANCED
SCIENCE NEWS**

www.advancedsciencenews.com

**steel
research**
international

www.steel-research.de

Figure 1. Mold sub-surface temperature 3D contour plot using hot color map with (a) and without (b) grid spacing conveying spatial information.

4. Color Map Selection for Scalar Fields

Color map selection can be a surprisingly complex task which often requires balancing a variety of conflicting goals such as user preference, standard convention, and practicality.[11,12] There are many color maps in existence today, and substantial discussions in the literature with regard to efficacy.[13] What is generally agreed upon, is that some color maps are better than others at conveying particular types of data, and if care is not taken, it is easy to choose poorly.[14]

Color map selection is often chosen with little thought, taking the software default during post processing of data. While taking the default color map might be an easy choice, it is often not the best for conveying the particular information at hand. Stopping for a moment to consider other color-map options can be very beneficial.

For many applications that involve temperature, including steel continuous casting, one of the most intuitive and useful color maps is blackbody radiation (called "hot" in MATLAB or "hot", "gist_heat", or "afmhot" in matplotlib). This color map is derived from the colors emitted due to black body radiation from a hot object at elevated temperature. The exact wavelengths of light observed in nature are adjusted to have a constant increase in brightness throughout and to be perceptually uniform. Liquid (or the hottest color of interest) is usually denoted as white, while the darkest solid is denoted as black. The contrast allows for easy understanding of the temperature field, and its physical basis makes it intuitive, because it matches human experience.

Rainbow color maps are popular, perhaps because of the misconception that the range of colors is complete, enabling the widest possible range to convey the data. However, research has repeatedly shown that the rainbow color map is rarely the optimal choice for data display due to: its tendency to confuse natural perceptual ordering, its uncontrolled luminance variation, and its regions with limited perceptual change, but significant change in represented value.[15] **Figure 2** shows the same 2D temperature data set shown in Figure 1 using four different color maps, plotted with MATLAB.[9] While it is still possible to discern [temperature] changes and trends in the rainbow (b) and hsv (c) color maps, it is far less intuitive than the blackbody (a) and gray (d) maps.

Publications often do not allow for color figures in print, and if researchers download and print articles they may not have easy access to a color printer. Thus it is important to consider how figures will appear in black and white, and to ensure that they still convey the intended information.

Continuously-changing color maps can be difficult to read accurately, because it is difficult for the human eye to distinguish between subtle changes in color. Instead, using discrete bands, sometimes referred to as "color banding," can provide distinct, thin boundaries between the colored regions, which correspond with specific values given in the legend. In addition to enabling more accurate reading of the contour map, these lines may also have physical significance. For example, each color in **Figure 3** represents a different material phase, so the contour lines represent phase-change interfaces.

Using discrete and obviously different colors to distinguish regions, certain times heavy contrast is desired and makes choosing colors across the spectrum not only helpful, but often preferred. Figure 3 shows phase fraction and temperature results from a 2D Lagrangian solidification model of longitudinal depression formation; details of this model can be found elsewhere.[16,17]

This custom color map was chosen for intuitive reading and understanding. The two highest temperature regions both contain liquid and are given colors with higher perceived temperatures (red and yellow). Red and yellow were chosen over orange to accentuate the change in phase more clearly. The lower temperature, fully solid regions, use cooler perceptual colors (green, teal, and blue), again chosen to be different enough to provide contrast accentuating the different phases. The displacements are scaled 5x equally in both X and Y in order to see the surface depression shape more clearly, while preserving the aspect ratio of all of the layer thicknesses as well as the surface depression shape. Finally, a thin vertical line shows the symmetry plane.

Commercial packages which feature results presentation, such as ABAQUS,[18] ANSYS Fluent,[19] matplotlib,[20] Para-View,[21] MATLAB,[9] and Tecplot[22] are excellent tools when used properly. However they can produce confusing results as a consequence of non-optimal post processing decisions, such as unfortunate choices for color maps and plot colors. Each
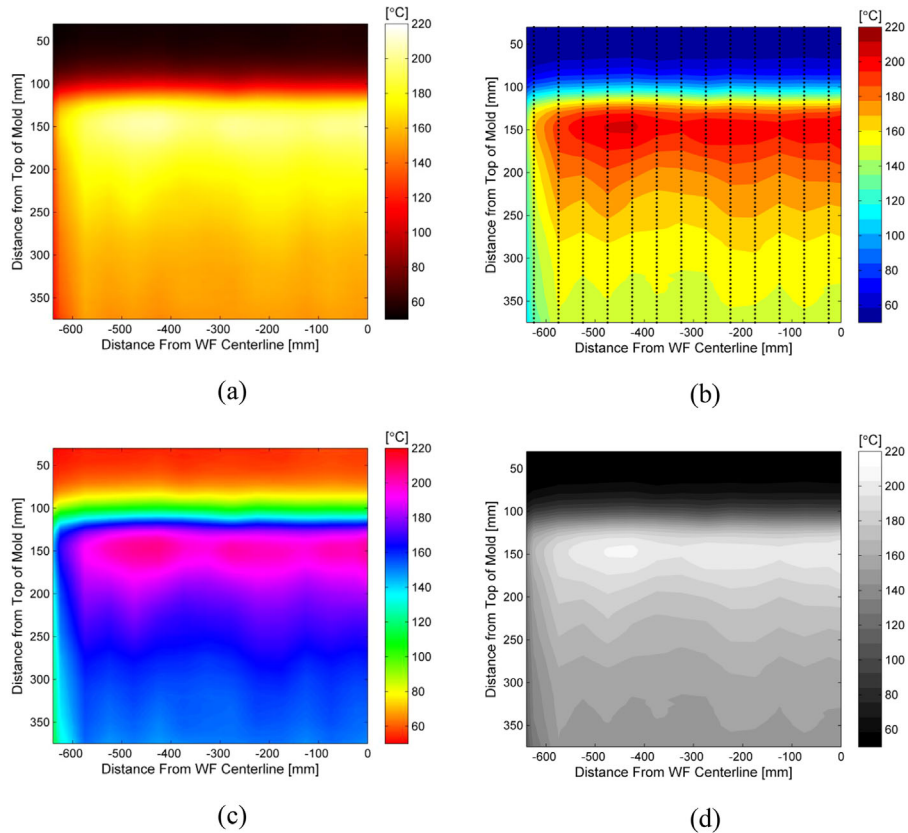
**ADVANCED
SCIENCE NEWS**

www.advancedsciencenews.com

**steel
research**
international

www.steel-research.de

Figure 2. Two-dimensional contour plots of mold sub-surface temperature in various MATLAB color maps: a) hot (blackbody radiation), b) jet (rainbow), c) hsv (rainbow color map in HSV space), and d) gray (grayscale).

program is capable of applying good color maps, but taking the default is rarely the best method for conveying results.

5. Vector-Field Representation

Vector field plots of velocity are very useful together with scalar-field color plots to accurately visualize complex physics phenomena, such as thermal fluid flow, particle transport, and magnetohydrodynamics in the mold and strand regions of a steel continuous caster. Presenting 3D vectors in a 2D presentation medium, which is common for Computational Fluid Dynamics (CFD) results, requires careful choice of cross sections and views. One approach is to construct a series of 2-D cross-sections through the 3D domain, viewed orthonormally

(aligned with a coordinate axis), to enable easier extraction of quantitative values from the contours, vectors, and streamline plots. For example, **Figure 4** shows an isometric visualization which includes several important 2-D cross sections with 2-D contour plots of temperature and velocity magnitude, the latter superimposed on velocity vectors. It was created by extracting results from a 3D thermal fluid flow analysis of a particular continuous caster using ANSYS Fluent[19] and taking advantage of symmetry to construct views of different fields in each mold half, using Tecplot.[22] To focus on important regions related to understanding the flow field and defect formation, five different cross-sectional planes are shown: the center middle plane between wide faces, two vertical planes, taken 10 mm from the steel shell front on the two narrow faces, and three horizontal
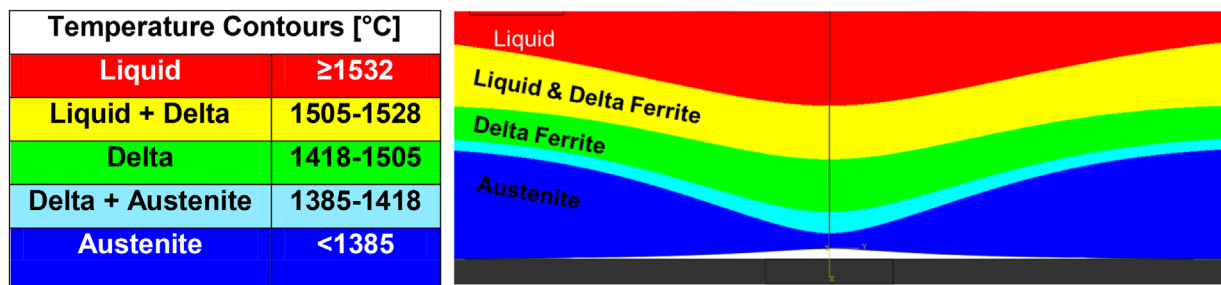

Temperature Contours [°C]	
Liquid	**≥1532**
Liquid + Delta	**1505-1528**
Delta	**1418-1505**
Delta + Austenite	**1385-1418**
Austenite	**<1385**

Figure 3. Longitudinal depression finite element solidification model 2D contour plot showing temperature and phase fraction (deformation scaled 5x).

**ADVANCED
SCIENCE NEWS**

www.advancedsciencenews.com

**steel
research**
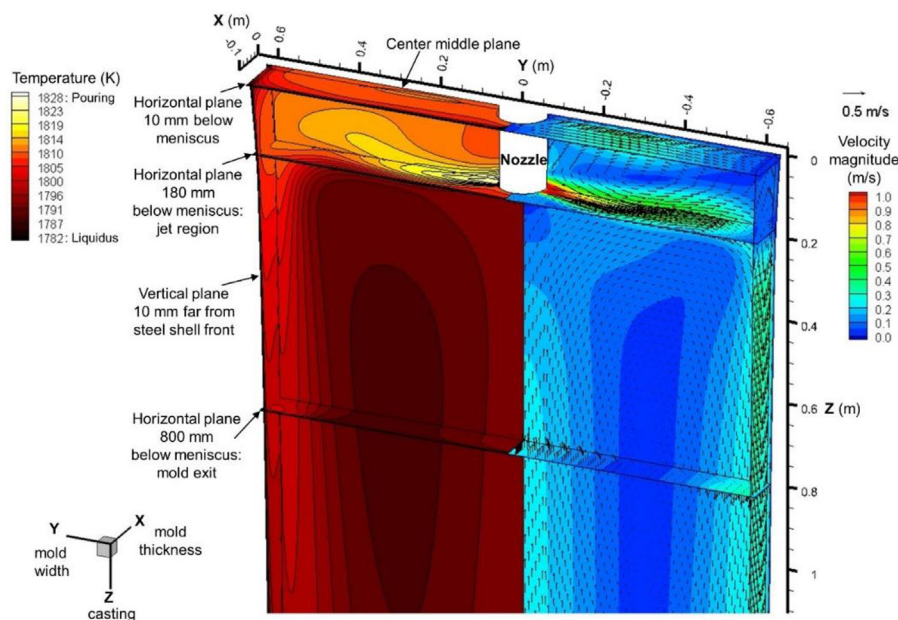international

www.steel-research.de

Figure 4. 3D visualization of thermal fluid flow fields in mold region during continuous steel-slab casting.

planes (10 mm (top), 180 mm (jet region), and 800 mm (mold exit) below the top surface meniscus) in the 3D model domain. The latter three planes show the jet shape, slag entrainment, entrapment, and initial solidification at the meniscus top surface, and the mold exit region, where excessive flow can cause a shell-thinning breakout. Thus, in this figure, the jet flow pattern can be seen, as well as its effect on temperature distribution inside the mold cavity, and the entrainment of slag to form defects near the top surface.

6. Tensor-Field Representation with Divergent Maps or Glyphs

Stress and strain at a point is represented by a tensor with up to six unique values associated with each variable in a three dimensional analysis. Combined with three unique displacement fields, this makes visualizing the results of a stress analysis a challenge. To help with this, variables which combine components together in physically relevant ways have been created, such as Von Mises stress (to be compared with yield stress for ductile failure), principal stresses (to be compared with fracture stress for brittle failure), and the corresponding strains. However these new fields create additional variables to convey. Thus, multiple contour plots, using different orientations and different stresses, are usually required to understand the particular problem at hand. Another important attribute of variables such as stress and strain is that data values often take on positive and negative values. Visualizing results is different for this situation, owing to the common need to indicate the significant qualitative change in the results that takes place at zero.

Sometimes, it helps to convey this data using glyphs to show multiple components of the stress tensor at a given point.[23] As shown in **Figure 5**a,[24] a black and white figure with simple glyphs can accomplish the same thing as several full color

contour plots. At each point in this figure, the principal tensile stress is shown as a line, and the principal compression stress as a line with tic-marks, oriented on new coordinate directions rotated to the appropriate angle for zero shear in the given horizontal plane of interest. The Von Mises effective stress is shown in Figure 5b, with a sign applied according to the largest magnitude stress in order to visualize regions of tension and compression. When used properly, glyphs are a useful method to convey data with limited space and/or color resolution.

Another way to handle the qualitative change at zero is via a "diverging" color map; where a dark color is chosen for each end of the map and blends to a neutral color (usually white) at the center.[25] To properly convey the qualitative change, it is important that the color map diverges (is centered) around zero. This can be a challenge when the positive and negative values are not equal in magnitude which may cause the similar colors to indicate both a positive and a negative value (i.e., if in Figure 5c light blue and light red both indicated tension instead of compression and tension, respectively). To avoid this issue, shifting the color map "0 point" around is a common feature of many software packages.

In certain situations plotting stress using a color scale with limits that are too high can actually wash out the color change from truly useful data. As such, it is important to understand where global extrema values appear in the domain, as well as their magnitude in relation to the bulk behavior. Denoting extreme values as outliers in the map with black or white, or another value that obviously stands out in the color map, can help in this situation.

7. Thermal Integral Methodology

The extraction of knowledge contained in large data sets can be aided by enhancement of features or new variables which best
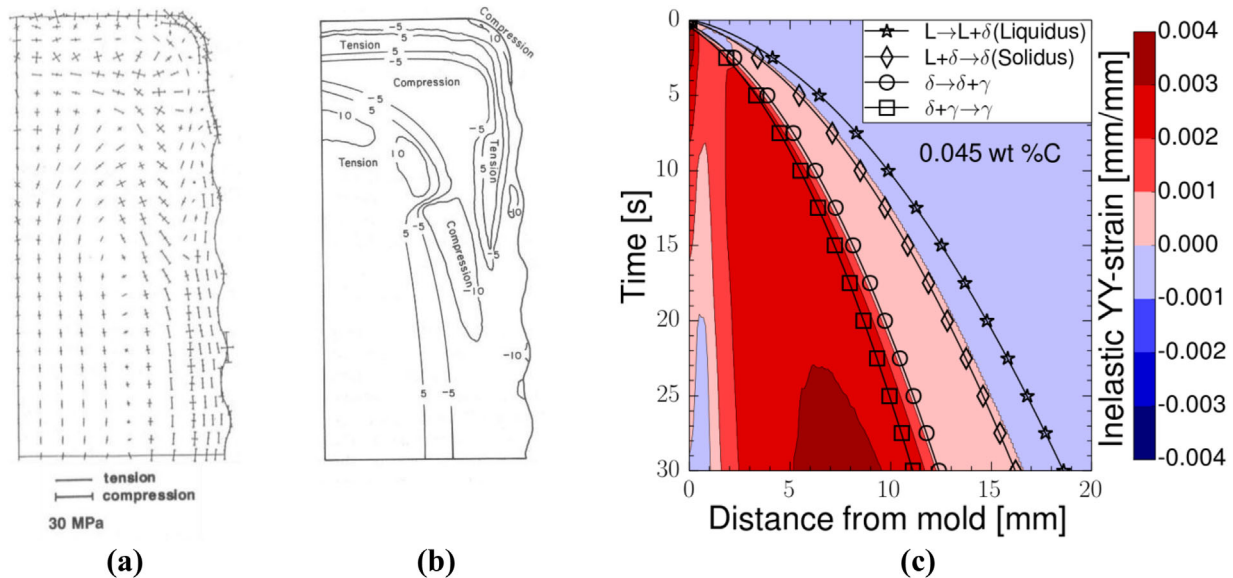
1800540 (5 of 11)

Figure 5. a) Black and white deformed shape contour plot showing deformation and stress using simple glyphs to convey tension and compression[24] reprinted with permission. b) The same deformed shape plot as (a) using numbered contour bands to convey tension and compression[24] reprinted with permission. c) Contour plot of inelastic strain using diverging color map with discrete bands oriented with red for tension and blue for compression.[26] Reprinted with permission.

convey that information. This section presents a new methodology to enhance the interpretation of continuous online measurement of dense mold temperature data to aid operators in detecting impending formation of longitudinal defects. Ideally, in continuous processes, such as the continuous casting of steel, conditions should remain constant at essentially steady state. In reality, changes are always occurring on many different time scales, and the operation can be transient in many different ways. It is important to know when such changes are normal, or when they are significant and worsening, requiring corrective action by the operator. Thus, caster operations at all plants provide monitors to show the operator many important process variables and their thresholds or limits which are often portrayed as lines across the top and bottom of the screen, to convey the windows of acceptable operation to stay within. Typical variables include casting speed, mold heat flux, steel composition aims, tundish superheat, SEN submergence, level profile in the mold to convey level fluctuations, spray water flow rates, and surface pyrometer temperatures. These metrics, and the differences between the current value and the acceptable thresholds, are tracked during casting and examined continuously in the operation pulpit.

Quality during continuous casting is greatly affected by heat transfer across the interfacial gap between the copper mold walls and the steel strand, which governs initial solidification of the steel shell and the formation of surface cracks and other defects.[16,17,27] Previous work has shown that cracks correlate with high and/or variable heat flux in the mold, especially near the meniscus region.[28] Thus, quality monitoring systems routinely include the measured mold heat flux signal, based on heat up of the cooling water as it passes through the mold[29,30] as well as other methods.[29,31,32]

Recently, it has become possible to obtain dense temperature measurements in the mold. This is accomplished with Fiber

Bragg Gratings, which can measure temperature at more than 2000 locations within the mold using fibers embedded inside the copper plates.[33,34] Though manufacturing and maintaining these specialized molds is complex, numerous advantages over traditional thermocouples are seen, particularly faster response time, and smaller spacing between sensors, which enables the presentation, in real time, of transient temperatures within the mold in higher resolution.[35,36]

An example of an instantaneous temperature profile measured across the mold subsurface is shown in **Figure 6**. The resolution of the data is indicated by the straight line segments plotted between measured points, which are sufficiently dense to capture the real profile behavior under most conditions. This figure also shows two horizontal lines, which represent the typical average of temperatures measured for this
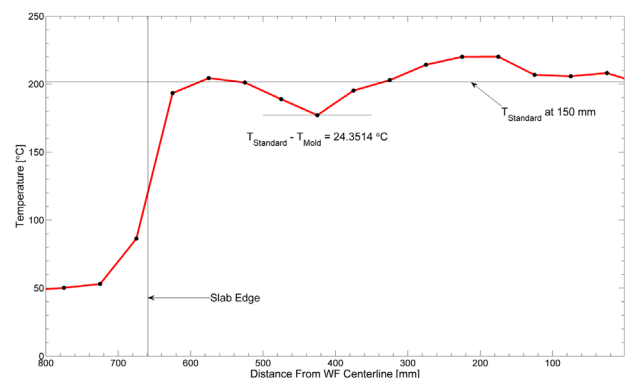

Figure 6. Measured local temperature profile and an example standard temperature profile 150 mm below top of mold from wide face centerline to slab edge.

**ADVANCED
SCIENCE NEWS**
www.advancedsciencenews.com

**steel
research**
international

www.steel-research.de

steel grade at this casting speed at this distance down the mold, and the local minimum.

One of the purposes of displaying the evolving temperature map is to enable operators to spot the formation of slab surface defects such as longitudinal depressions and cracks during residence time in the mold. In addition to mechanical conditions, their formation is often linked to thermal variations, usually, reductions in heat transfer. Reduction in heat transfer within the mold region leads to elevated temperatures on the surface of the slab, and lower temperatures seen by the mold surface when these defects are present. These defects typically form close to the meniscus, and grow as they move vertically down the mold at the casting speed.[37] This motion suggests a physically-based methodology to improve understanding of the resultant signals.

Specifically, the relative drop within the entire instrumented region of the mold between the standard temperature profile and the instantaneous temperature profile summed according to the residence time of the slab surface at that location down the mold.

7.1. Mapping Mold Data to Slab Data

There is a unique spatial and temporal mapping of mold temperature data, $T_{Mold}(x_{Mold}, y_{Mold}, t)$, to slab temperature, $T_{slab}(x_{Slab}, y_{Slab}, t)$, according to the time, location, and casting speed history. As shown in **Figure 7**, y_{Mold} is the distance up the mold subsurface from the reference location, y_{mold0}, which is located at the bottom of the instrumented region where temperature data is measured; and y_{Slab} is distance along the slab, opposite to the casting direction, from y_{Slab0}, which is a reference location fixed on the slab that aligns with the bottom of the instrumented region at the reference starting time, ($y_{Slab} = y_{Mold}$ at $t = t_0$). For a given mold, the horizontal locations on the slab and mold, measured from a fixed horizontal reference such as the mold centerline, are identical, $x_{Slab} = x_{Mold}$.

At any given time, t, the vertical location of any specific point of interest down the slab surface, y_{Slab}, is related to the point in

Figure 7. Nomenclature for mold and slab geometry reference configuration used in Integral Defect methodology (shown at t_0).

the mold it is currently adjacent to, y_{Mold}, according to:

$$y_{Slab}(t) = y_{Mold} + \int_{t_0}^{t} V_c(t_i)dt_i \tag{1}$$

where the last term in this equation is the vertical distance traveled downward by the slab location since the reference starting time at t_0, and V_c, is the casting speed, which also may vary with time.

For a constant casting speed Equation (1) simplifies to:

$$y_{Slab}(t) = y_{Mold} + V_c^*(t - t_0) \tag{2}$$

Mapping mold temperature to slab temperature, according to Equation (1) gives:

$$T_{slab}(x_{Slab}, y_{Slab}, t) = T_{Mold}\left(x_{Mold}, \ y_{Mold} + \int_{t_0}^{t} V_c(t_i)dt_i, \ t\right) \tag{3}$$

7.2. Defect Criterion

The following criterion helps to identify cracks and other defects associated with longitudinal depressions by indicating regions on the strand surface that have experienced multiple, or prolonged, periods of temperature drops relative to the standard profile. The drop in the current temperature at any given measured point in the mold subsurface, relative to the standard temperature at that location is

$$\Delta T(t) = \min(0, T_{Mold}(x_{Mold}, y_{Mold}, t) \\ - T_{Standard}(x_{Mold}, y_{Mold}) + a) \tag{4}$$

where $T_{Standard}$ is a 2D array of standard temperatures at the instrumented points of the mold, calculated previously by averaging data when no defects occurred, according to the given steel grade and casting conditions. The constant, a, is a threshold value that could be used to filter random variations in T (currently set to 0). This criterion ignores temperature increases, because they are not believed to help heal any defect that may have formed.

Inserting Equation (3) into Equation (4) gives:

$$\Delta T(t) = \min\left(0, T_{Mold}\left(x_{Slab}, y_{Slab} - \int_{t_0}^{t} V_c(t_i)dt_i, t\right) \\ - T_{Standard}\left(x_{Slab}, y_{Slab} - \int_{t_0}^{t} V_c(t_i)dt_i\right)\right) \tag{5}$$

While a location of interest on the slab surface, y_{Slab}, is within the instrumented region of the mold, $t_{Enter} < t < t_{Exit}$, the criterion, T_{IDrop}, evolves with time by integrating the history of the temperature drop at that moving location:

$$T_{IDrop}(x_{slab}, y_{slab}, t) = \int_{t_{Enter}}^{t} \Delta T(t_i)dt_i \tag{6}$$

where t_{Enter} is the time when the location, y_{Slab}, enters the instrumented mold region, $y_{Slab} = y_{MoldTop}$. This time is typically known from recorded data for the slab, heat, and time and can also be calculated using the reference time, t_0, the length of the
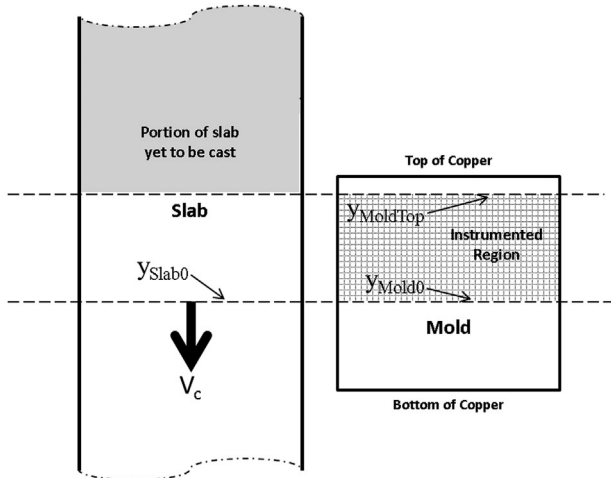
instrumented region, $\gamma_{MoldTop}$-γ_{Mold0}, and the casting speed history:

$$\gamma_{Slab} - \gamma_{MoldTop} = \int_{t_0}^{t_{Enter}} V_C(t_i)dt_i \qquad (7)$$

For a constant casting speed, this simplifies to:

$$t_{Enter} = t_0 + \frac{\gamma_{Slab} - \gamma_{MoldTop}}{V_C} \qquad (8)$$

Once the location of interest, γ_{Slab}, passes out of the instrumented region, $\gamma_{Slab} \geq \gamma_{Mold0}$, at time, $t \geq t_{Exit}$, $T_{IDrop}(x_{slab}, \gamma_{slab}, t)$ is no longer time dependent and its final constant value, $T_{IDropF}(x_{slab}, \gamma_{slab})$ is found by setting $t = t_{Exit}$ in Equation (6), where t_{Exit} is the time when the location of interest reaches the last instrumented point in the mold.

$$\gamma_{MoldTop} - \gamma_{Mold0} = \int_{t_{Enter}}^{t_{Exit}} V_C(t_i)dt_i \qquad (9)$$

For a constant casting speed, and knowing t_{Enter} from Equation (7), Equation (9) simplifies to:

$$t_{Exit} = t_{Enter} + \frac{\gamma_{MoldTop} - \gamma_{Mold0}}{V_c} \qquad (10)$$

7.3. Implementation and Interpretation

The equations given in the previous section are well suited for computational implementation. For an arbitrary casting speed history, Equation (7) and (9) each require solving a definite integral for the upper integration limit. This is readily accomplished with an incremental time-marching procedure. Similarly, Equation (6) can be represented as a summation:

$$T_{IDrop}(x_{slab}, \gamma_{slab}, t) = \sum_{t=t_{Enter}}^{t_{Exit}} \Delta T(t) \qquad (11)$$

and after substituting in Equation (5), Equation (11) gives:

$$T_{IDropF}(x_{slab}, \gamma_{slab}, t)$$
$$= \sum_{t=t_{Enter}}^{t_{Exit}} \min(0, T_{Mold}(x_{Mold}, \gamma_{Mold} + \int_{t_0}^{t} V_c(t_i)dt_i, t)$$
$$- T_{Standard}(x_{Mold}, \gamma_{Mold} + \int_{t_0}^{t} V_c(t_i)dt_i)) \qquad (12)$$

The definite integrals contained within Equation (12) can again be solved incrementally. As Equation (11) is evaluated for a location of interest, γ_{Slab}, at increasing time, t, (using constant time steps of 1 s in this work) the value of T_{IDrop} at each point on the slab surface, starting at zero, evolves with time while moving through the instrumented region, and retains its final value upon exiting that region, T_{IdropF}.[38]

According to this criterion, only temperature drops contribute to the integral, as temperature increases are believed not to cancel out previous temperature drops.[16,38] A low heat flux, followed by a return to "standard" heat flux at a given location on the slab surface, is better than staying below the standard for a prolonged period, which is reflected in a lower value of T_{IDropF}. However, actually increasing above the standard profile is not likely to compensate for prior decreases. On the contrary, such increases might further exacerbate defect formation, as previous work has correlated mold temperature fluctuations with increasing incidence of transverse[30] and longitudinal[39] crack and depression appearance. Previous work is based only on particular locations in the mold however, as strand movement has not been taken into account in a defect criterion before T_{IDropF} in the current work.

Large values of T_{IDropF} indicate regions of the slab surface which have experienced a mold temperature history that is cooler than standard conditions. This indicates lower heat flux across the interfacial gap and a hotter shell temperature. While low heat flux can occur due to local mold slag variations, it is often due to surface depressions, sometimes including an air layer within the interfacial gap between the shell and mold. These low heat flux depression regions see higher slab surface temperature and often lead to cracks. These regions can be tracked, subjected to extra inspection, and perhaps downgraded. This methodology and criterion can be applied to systems with arbitrary spacing of the measurement points, provided there is enough spatial resolution to achieve reasonable accuracy.

The result of Equation (12), T_{IDropF}, is a 2D array of values representing the accumulated temperature drop of each location on the slab surface as it passes through the instrumented mold region. When plotted properly, as in **Figure 8**d, this contour map indicates regions on the strand surface that have experienced multiple, or prolonged, periods of temperature drops relative to the standard profile.

8. Results

An example of an instantaneous snapshot of all of the measured data recorded in one wide face of the mold, using a continuous, blackbody, temperature map is shown in Figure 8a. This temperature map provides a more direct local indication of heat transfer across the interfacial gap. However, the 2D contour plot creates a new problem, as the operator is challenged to perceive any important differences between the current values, and threshold limits, which no longer can be included as bounding lines on the top and bottom of a single time-evolving signal.

To resolve this problem, the current work proposes a direct portrayal of the differences between the current and standard conditions, magnified to facilitate the visualization of defect formation. This is difficult for several reasons. In display of the current signal, one might be tempted to filter out the noise (small fluctuations in temperature), to make real "large" variations easier to perceive. However, some of the small changes actually contribute valuable information. The second challenge is to find

**ADVANCED
SCIENCE NEWS**

www.advancedsciencenews.com

**steel
research**
international

www.steel-research.de

a reasonable set of standard conditions, as displaying a range is no longer an option. Finally, augmenting the difference between current and standard conditions requires knowing which differences are real, based on the reason that they are being displayed.

Figure 8a–d shows a recommended console display setup for post-mortem (forensic) defect analysis using this new defect indicator applied on half of the continuously cast slab. Figure 8a–c share a common y-axis spanning the 345 mm instrumented region within the mold, while this same region is represented between the thick horizontal lines in Figure 8d. Figure 8a shows the instantaneous contour map in the instrumented region collected by the sensors at the current time, using the blackbody color map without interpolation. It is important that this contour map use strictly linear interpolation, other methods risk creating artificial over- and under-shoots of the data. These extrema may accidentally wash out issues with sensors or other problems and distract from the more subtle changes which are the real temperature deviations.

Figure 8b shows a top-down photograph (adjusted to remove perspective) of the final surface appearance of the region of the cast slab corresponding to the temperatures in Figure 8a at the time it matched the instrumented region in the mold. The translucent gray rectangle at the top indicates that portion of the image which was above the meniscus level at that time. While this image requires careful reconstruction, seeing how the measured temperatures line up with eventual surface quality problems is a helpful means of using this methodology to elucidate how defects form. Once this has been accomplished, and the results map in Figure 8d has been determined to properly indicate defects, according to downstream product evaluations, then a real-time version of this display in the mold can be created, without Figure 8b. This would enable operators to make decisions in real time to correct evolving surface defects apparent in the results map.

Figure 8c shows a linearly interpolated contour plot of the instantaneous deviations between the standard and current temperatures for each location in the array. Values on this plot naturally always have a negative or zero value, as discussed previously. Zero indicates that temperature history experienced at that location was within the specified threshold of the standard temperature profile. Increasingly negative values indicate larger temperature drops.

Figure 8d shows an example of the output results from this methodology, obtained by accumulating the results in Figure 8c for 11 s (245 mm past the bottom of the instrumented region), according to the new defect criterion function in Equation (6). The time period spent within the instrumented region of the mold is represented by the space between the thick black horizontal lines labeled top and bottom of instrumentation. Once a surface location passes out of the instrumented region, the contours are fixed, and the calculation for that surface point is completed; in the video this can be seen by the data in Figure 8d compressing in the y-direction. Values in this contour plot also take on a negative or zero value, where increasingly negative numbers indicate higher likelihood of surface quality problems. The longitudinal depression seen at the bottom left of Figure 8b is clearly visualized in Figure 8d, while it is hardly noticeable in the raw temperature data in Figure 8a. A video of Figure 8 found in the supplemental files provides further detail.

9. Discussion

For online operation in real time, a streaming image taken with laser or optical scanners (either of the slab surface shape exiting the caster, or of the rolled coil) might be matched with the corresponding mold temperature images taken previously and offset, and be used to evaluate quality and dispositioning (shipping or downgrading) of the steel product. The new images
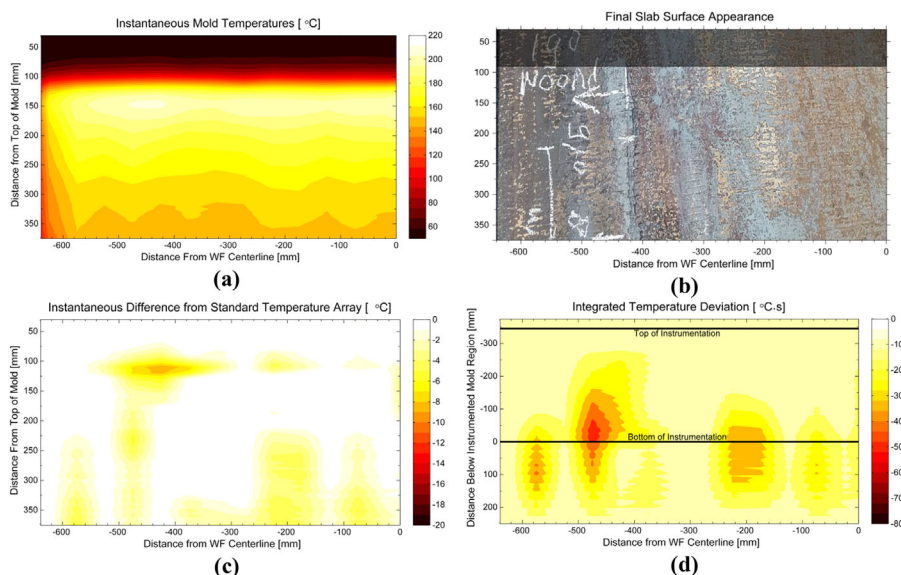

Figure 8. Contours indicating defects mapped over half of slab from wide face centerline to narrow face: a) Instantaneous mold temperature, b) Final slab surface appearance, c) Instantaneous difference from standard temperature. d) Defect criterion based on integrated temperature drop, T_{IDropF}.

showing the integrated temperature drops could be helpful in the determination of slab or coil downgrading.

This method tracks small temperature changes, so the standard profiles are very sensitive to casting conditions: grade being cast, casting speed, superheat, mold powder, mold geometry, and flow conditions, which vary from caster to caster. In addition to careful tracking and updating of the averages which represent standard conditions, natural variations not related to defect formation may need to be filtered, which would require adjusting the threshold temperature drop, a.

High thermal gradients near the meniscus region and near the slab corners make these areas very sensitive to minor temperature variations. Although level fluctuations may contribute to surface quality problems, their effects cause large T_{IDrop} values across the top of the mold. Similarly, the cooler corners cause large T_{IDrop} values down the region adjacent to the narrow face edges, especially when automated width changes and sensor spacing issues make the exact location of the corner difficult to determine. For these reasons it was found necessary to truncate the top and side portions of the instrumented region, only using data below the meniscus at y_{Enter}, and away from the narrow faces.

Depending on the depth and response time of the temperature measurements, further tuning may be needed to implement this methodology into a given steel plant. The new field variable, T_{IDropF}, requires sufficiently high density thermal data collection in the mold to capture the thermal signature of the strand surface defects. A set of only a few rows of breakout detection thermocouples in the casting direction does not provide enough information/history for each discrete slab location to produce accurate results.

10. Conclusions

Post processing and visualization of results is a crucial aspect of computational modeling and analysis of sensor data. If done correctly, substantial amounts of information can be condensed into a few simple images or videos to convey the important insights into the process. In this work, some recommendations are made for color maps, viewing orientations, and other aspects of visualization of 2D and 3D results relevant to materials processing, including scalar field variables such as temperature, vectors such as velocity, and tensors such as stress. In most cases, a default rainbow color map is not as intuitive as data-specific color map, such as blackbody radiation for temperature and diverging Red-Blue for stress. Finally, a new methodology is introduced to visualize defect formation from high density temperature data recorded in a continuous casting mold. The likelihood of surface quality problems can be predicted based on an integrated temperature drop relative to a standardized temperature profile, T_{IDropF}. When calibrated properly, this method can enable real time monitoring of surface quality issues inside the mold during commercial continuous casting processes.

Conflict of Interest

The authors declare no conflict of interest.

[1] S. Cho, B. G. Thomas, S. Kim, *Metall. Mater. Trans. B* **2018**, 2651, 1.
[2] B. G. Thomas, Q. Yuan, S. Sivaramakrishnan, S. P. Vanka, *J. Met. (JOM-e)* **2002**, *54*, 20.
[3] B. G. Thomas, Q. Yuan, B. Zhao, S. P. Vanka, *J. Met. (JOM-e)* **2006**, *58*, 16.
[4] K. Timmel, S. Eckert, G. Gerbeth, *Metall. Mater. Trans. B* **2011**, *42*, 68.
[5] M. M. Salazar-Campoy, R. D. Morales, A. Nájera-Bastida, I. Calderón-Ramos, V. Cedillo-Hernández, J. C. Delgado-Pureco, *Metall. Mater. Trans. B* **2017**, *48B*, 1376.
[6] K. Jin, S. P. Vanka, B. G. Thomas, *Metall. Mater. Trans. B* **2018**, *49*, 1360.
[7] J. Sengupta, H. J. Shin, B. G. Thomas, S. H. Kim, *Acta Mater.* **2006**, *54*, 1165.
[8] J. Sengupta, B. G. Thomas, *J. Met. (JOM-e)* **2006**, *58*, 16.
[9] Mathworks, MATLAB - Mathworks - MATLAB & Simulink. **2016**.
[10] P. M. Gresho, R. L. Lee, *Comput. Fluids* **1981**, *9*, 223.
[11] A. C. Telea, *Data Visualization - Principles and Practice*, 2 edn., CRC Press, Boca Raton, FL, USA **2014**.
[12] L. D. Bergman, B. E. Rogowitz, L. A. Treinish, *Proc. 6th IEEE Vis. '95*, IEEE, Piscataway, NJ, USA **1995**, 118.
[13] L. Zhou, C. D. Hansen, *IEEE Trans. Vis. Comput. Graph.* **2016**, *22*, 2051.
[14] K. Moreland, *IS&T International Symposium on Electronic Imaging.* Society for Imaging Science and Technology (IS&T), Springfield, VA. USA **2016**, P. HVEI-133.1.
[15] D. Borland, R. M. Taylor, *IEEE Comput. Graph. Appl.* **2007**, *27*, 14.
[16] M. L. S. Zappulla, B. G. Thomas, *THERMEC' 2018, Paris, Mater. Sci. Forum* **2018**, *941*, 112.
[17] M. L. S. Zappulla, B. G. Thomas, *TMS 2017 146th Annual Meeting Suppl. Proc., TMS* **2017**, *Part F6*, 501.
[18] ABAQUS, ABAQUS 6.13 Verification Manual. DS SIMULIA Corp, **2013**.
[19] ANSYS Inc., Fluent User Manuals. **2016**.
[20] J. D. Hunter, *Comput. Sci. Eng.* **2007**, *9*, 90.
[21] A. Henderson, *The ParaView Guide: A Parallel Visualization Application*, Sandia Natl Lab, Los Alamos, NM **2004**.
[22] Tecplot Inc., Tecplot 360 EX User's Manual. **2018**.
[23] Y. M. A. Hashash, J. I. C. Yao, D. C. Wotring, *Int. J. Numer. Anal. Methods Geomech.* **2003**, *27*, 603.
[24] B. G. Thomas, I. V. Samarasekera, J. K. Brimacombe, *Metall. Mater. Trans. B* **1987**, *18B*, 131.
[25] K. Moreland, *5th Int. Symp. ISVC 2009*, Springer-Verlag, Berlin **2009**, p. 92.

[26] M. L. S. Zappulla, L. C. Hibbeler, B. G. Thomas, *Metall. Mater. Trans. A* **2017**, *48*, 3777.

[27] M. L. S. Zappulla, *M.S. Thesis*, Univ. Illinois, Urbana, IL, **2016**.

[28] M. Kawamoto, Y. Tsukaguchi, N. Nishida, T. Kanazawa, S. Hiraki, *ISIJ Int*. **1997**, *37*, 134.

[29] Y. Zhang, V. Vaculik, M. Dudzic, *IFAC Proc*. **2003**, *36*, 561.

[30] S. Kumar, J. A. Meech, I. V. Samarasekera, J. K. Brimacombe, V. Rakocevic, *Ironmaking Steelmaking* **1999**, *26*, 269.

[31] W. H. Emling, in *Making, Shaping, and Treating of Steel - Casting* (Ed: A. W. Cramb), AISE Steel Foundation, Warrendale, PA **2003**.

[32] G. O. Tirian, I. Filip, G. Proştean, *Neurocomputing* **2014**, *125*, 236.

[33] T. Spierings, A. Kamperman, H. Hengeveld, J. Kromhout, E. Dekker, *AISTech 2017 Proc*., AIST, Warrendale, PA **2017**, p. 1655.

[34] G. Hedin, A. Kamperman, M. Seden, K. Frojdh, J. Pejnefors, *SCANMET V: 5th International Conference on Process Development in Iron and Steelmaking*, Swerea MEFOS, Luleå, Sweden June 12-15, **2016**.

[35] A. B. Badri, A. W. Cramb, in *Steelmak. Conf. Proc*. Iron Steel Soc. (AIST), Warrendale, PA **2002**, p. 65.

[36] B. G. Thomas, M. Okelman, in *Sensors, Sampling, and Simulation for Process Control*, TMS, Warrendale, PA. **2011**, p.127.

[37] S. Kumar, B. N. Walker, I. V. Samarasekera, J. K. Brimacombe, *13th PTD Conf. Proc*., AIST, Warrendale, PA **1993**, p. 119.

[38] M. L. S. Zappulla, *Colorado School of Mines*, CCC Annual Report, **2018**.

[39] D. Stewart, P. N. Hewitt, L. Peeters, *Steelmak. Conf. Proc*. Iron Steel Soc. (AIST), Warrendale, PA **1996**, p. 207.